Research Article

Journal of Environmental Nanotechnology

Thermal and Mechanical Performance of Ultra-high-performance Basalt Fiber Concrete Incorporating Nano Agricultural Waste Additives at Ambient and Elevated Temperatures

Ananthakumar Ayyadurai[1*], M. M. Saravanan[1], G. Dineshkumar[2], G. Viswanathan[3] and P. Easwaran[3]

[1]Department of Civil Engineering, Vivekanandha College of Engineering for Women, Tiruchengode, Namakkal, TN, India
[2]Department of Civil Engineering, Vaagdevi college of Engineering, Warangal, TG, India
[3]Department of Civil Engineering, Vivekanandha College of Technology for Women, Tiruchengode, Namakkal, TN, India
Received: 06.10.2025 Accepted: 29.01.2026 Published: 30.03.2026
*ananthaakumar7410@mail.com

ABSTRACT

This study explored the development of sustainable ultra-high-performance basalt fiber high-strength concrete (UHPBF-HSC) using agricultural waste materials. Nano-sugarcane bagasse ash (NSCBA), nano cotton straw ash (NCSA), and nano rice straw ash (NRSA) were incorporated as partial cement replacements. Additionally, basalt fiber (1.5%), silica fume (10%), and superplasticizer (0.5%) were consistently included in all mixes. The nanoparticles were produced through mechanical processing and heat treatment. Four dosage levels (5-20% by weight of cement replacement) were tested in combination with basalt fibers. The study evaluated the effects of elevated temperatures (300°C and 600°C) on UHPBF-HSC, focusing on compressive strength (CS), strength degradation, mass loss, ultrasonic pulse velocity, splitting tensile strength (STS), flexural strength (FS), and water absorption. Results indicated that increasing nanoparticle dosage generally enhanced mechanical properties. Among all mixes, the NSCBA4 (M4) mix exhibited superior performance, achieving approximately 9.7% and 23.0% higher CS than the corresponding NCSA4 and NRSA4 mixes, respectively, at identical replacement levels, in addition to outperforming conventional concrete. The mixes NCSA and NRSA showed similar performance but were less effective than NSCBA. Scanning electronic microscopic analysis revealed well-bonded matrices and compacted sections under normal conditions. However, elevated temperatures led to microcrack formation due to ettringite decomposition and water evaporation. A comparative analysis and prediction of STS and FS were conducted using various codes and literature sources.

Keywords: Nano-sugarcane bagasse ash; Nano cotton straw ash; Nano rice straw ash; Basalt fibers; Silica fume; Superplasticizer.

1. INTRODUCTION

The construction sector is focusing on reducing carbon emissions by using sustainable materials. One approach is the incorporation of agricultural by-products and industrial wastes into cementitious composites (Zeyad *et al.* 2024). Plant-based ashes including basil ash and sugarcane bagasse ash have demonstrated a high potential to serve as eco-friendly supplemental cementitious materials (SCM) which have led to reduction of waste, lowering of cement use and enhanced sustainability in concrete production (Anish *et al.* 2024; Perera *et al.* 2024). Such materials facilitate the development of green building technologies without compromising the mechanical performance. The ultra-high-performance concrete (UHPC) is known to have superior compressive strength (CS), dense microstructure, and excellent durability, and thus can be used in high and sophisticated structures (Abid *et al.* 2024, Hussain *et al.* 2024; Shi *et al.* 2024). Fiber content also adds to the UHPC, raising tensile strength, ductility and crack resistance. Basalt fibers (BF) have received growing popularity, thanks to their high tensile strength, thermo-resistance, resistance to corrosion, and the fact that they are eco-friendly as opposed to traditional steel fibers or synthetic fibers (Sun *et al.* 2024; Ünal *et al.* 2024). Basalt fiber-reinforced high-strength concrete has shown better mechanical performance and durability, especially in combination with SCMs and advanced mix designs (Supit *et al.* 2024; Muniyasamy *et al.* 2023; Zeyad *et al.* 2024). Recent research demonstrated that nanomaterials could be important in improving the working capacity of UHPC by fastening the cement hydration process, refining pore structure, and enhancing the bonding of fibers and the matrix (Althoey *et al.* 2023; Alomayri *et al.* 2023). Nano-scale additives, such as nano-silica and nano agricultural waste ashes, are effective and extremely beneficial in enhancing

compressive strength, tensile strength, flexural performance, and durability (Du *et al.* 2023, Ünal *et al.* 2023, Mostafa *et al.* 2022; Ubayi *et al.* 2024). Synergistic effect has also been reported when fibers and nanomaterials are used together, which create better mechanical properties and dense microstructures relative to traditional UHPC systems (Zheng *et al.* 2022; Nasser *et al.* 2022; Abbas *et al.* 2022).

Nano-sugarcane bagasse ash (NSCBA), nano cotton straw ash (NCSA) and nano rice straw ash (NRSA) are some of the agro wastes, that can be processed into nano-scale, where they exhibit high pozzolanic reactivity and a large specific surface area (Amin *et al.* 2021; Huang *et al.* 2021; Tran *et al.* 2021). The nano ashes increase the cementitious reactions, decrease porosity, and enhance the strength when incorporated as partial cement replacement in UHPC (Wijesundara *et al.* 2025; Yonggui *et al.* 2020). Previous research shows that sugarcane bagasse ash and other plant ashes can enhance the mechanical strength and durability of high-performance concrete when properly processed and incorporated (Berktaş *et al.* 2020; Zakare *et al.* 2020; Batool *et al.* 2020). A critical issue in the structural application of UHPC is its performance when exposed to fire or extreme temperatures. Exposure to high temperature may lead to loss of strength, loss of mass, and destruction of microstructure due to evaporation of moisture, decomposition of hydration products and formation of microcracks (Ahmed *et al.* 2008; Legeron *et al.* 2000). Basalt fibers are known to possess very good thermal resistance, and they are reported to increase mechanical properties and stability of UHPC when subjected to high temperatures (Ema *et al.* 2019; Chen *et al.* 1980). Nonetheless, research on the thermal and mechanical performances of UHPC due to the combined effect of basalt fibers and nano ashes of agricultural wastes is scarce. Although the literature on UHPC, nanomaterials, and fiber reinforcement is increasing, there are still gaps in the knowledge about the relative performance of various nano agricultural waste additives in basalt fiber-reinforced UHPC systems, especially at high temperature conditions (Carino *et al.* 1982; Oluokun *et al.* 1991; Khan *et al.* 2024; An *et al.* 2025; Almohammed *et al.* 2024; Saha *et al.* 2024; El *et al.* 2025; ACI 1997, ACI 1999, GB 50010-2010, 2015; Du, 2010; IS 56-2000). These gaps should be filled in to optimize the mix design and encourage practical implementation of sustainable UHPC materials.

Thus, the current research seeks to come up with sustainable ultra-high-performance basalt fiber high-strength concrete (UHPBF-HSC) utilizing nano agricultural waste materials, which are locally available. A total of 13 mixes of concrete were prepared containing a reference mix and four levels of replacement of each of the nano additives, NSCBA, NCSA, and NRSA. Fresh and hardened properties were tested, including compressive strength, splitting tensile strength, flexural strength (FS) and ultrasonic pulse velocity. The effects of the high temperature up to 600°C on the mechanical performance were also studied. Microstructural analysis of the optimal samples was also done to shed some light to the processes that control performance improvement and thermal degradation.

2. MATERIALS AND METHODS

2.1 Materials

In this study, Ordinary Portland Cement (OPC) of Grade 52.5 was used as a primary component of concrete. The specific gravity of the OPC was measured at 3.15, following the procedures outlined in IS: 4031 – 1988. The fineness and normal consistency of the OPC were found to be 6% and 31%, respectively. The setting times, crucial for construction applications, were recorded as 35 minutes for the initial set and 320 minutes for the final set. The CS of OPC 52.5 Grade was calculated to be 53.50 Mpa. The fine mix aggregate had a fineness modulus of 2.86, specific gravity of 2.56 and bulk density of 1680 kg/m^3. Coarse aggregates, which were made by crushing of stones were angular and all of similar size of 20 mm. Specific gravity of coarse aggregate was 2.68 (in compliance with IS: 383-1970) and the water absorption rate was 0.58%. The aggregate strength and crushing strength were 12.5% and 26.32%, respectively, according to the IS: 2386-1963 standards. Superplasticizers, which enhance the workability of concrete, were used in the study. The selected superplasticizer was naphthalene-based and met the standards specified in IS 9103-1999, BS: 5075 Part 3, and ASTM C-494. Additionally, basalt fibers with a length of 24 mm were incorporated, featuring tensile strength of 2.6 GPa, modulus of elasticity of 85 GPa, density of 2.65 t/m^3, elongation of 3.10%, and diameter of 16 μm.

The effects of NCSA, NRSA and NSCBA on the concrete properties were determined using nano-sized agricultural waste products. These were acquired from a village at Arunkulam, Thoothukudi District, Tamil Nadu, India. The agricultural residues were washed using tap water and dried in the air and subsequently burnt at 700°C to obtain amorphous silica-rich ash (Berktaş *et al.* 2020; Zakare *et al.* 2020). The resulting ashes were ground using high energy ball milling process and sieved to obtain the nano-sized particles.

Morphology and size of the nano materials were studied using Scanning Electron Microscopy (SEM) and Transmission Electron Microscopy (TEM). The particle diameter was calculated by direct measurements using TEM micrographs, and standard image analysis methods were applied. The results of TEM indicated that the mean particle sizes of NSCBA, NCSA and NRSA were approximately 81 nm, 47 nm and 60 nm, respectively. This demonstrated that the nano-sized particles had been produced successfully. The micrographs in Fig. 1 show

agglomerated and well-separated structures of NSCBA, NCSA and NRSA.

Table 1. Chemical composition of the raw materials

Component	Cement	NSCBA	NCSA	NRSA	SF
			Percentage (%)		
SiO_2	21.68	78.58	63.15	95.25	97.65
CaO	62.56	3.3	8.56	2.04	0.10
Al_2O_3	5.85	6.15	7.58	0.15	0.18
Fe_2O_3	2.61	3.52	4.75	0.16	0.19
Cl	0.06	0.03	0.03	0.98	0.02
SO_3	2.62	2.8	1.85	0.75	0.14
MgO	2.35	3.85	4.75	0.25	0.1
loss	2.27	1.76	9.32	0.42	1.62

The BET nitrogen adsorption analysis was applied to calculate the specific surface areas of the nano materials. The BET surface areas were measured at 1210 m^2/g in NSCBA, 1575 m^2/g in NCSA and 1441 m^2/g in NRSA. All these relatively high values can be explained by the nano-scale size of the particles, porous microstructure, and the high content of amorphous silica, caused by controlled combustion and intensive mechanical milling. The same trends of elevated surface area of nano-processed agricultural ashes have been described in previous research (Mostafa *et al.* 2022), implying that they are surface reactive which makes them potentially effective as supplementary cementitious additives. The selected exposure temperatures of 300°C and 600°C represent moderate and severe fire conditions, respectively, and are associated with critical thermal degradation levels of cementitious composites reported in the literature.

2.2 Concrete Mix Design

The experimental program was designed based on reference mixes established through a series of trials, aiming to develop a mix design that adheres to the European High-Performance Concrete (HPC) Guidelines 2004 (EN 206-1). The goal was to achieve a combination of ultra-high CS and desirable fresh concrete properties. As detailed in Table 2, thirteen concrete mixes were formulated to attain UHPBF-HSC grades. Each mix had a consistent binder content of 350 kg/m^3, with coarse aggregate and basalt fiber included at 1115 kg/ m^3 and 2.25 kg/ m^3 (1.5% by volume), respectively. These mixes were categorized into three groups. Group 1 (G1) involved replacing 5% to 20% of the cement with nano sugarcane bagasse, labeled M1 through M4. Group 2 (G2) similarly replaced 5% to 20% of the cement, but with nano cotton straw ash. Group 3 (G3) replaced 5% to 20% of the cement with nano rice straw ash. Each mix consistently included 10% silica fume. The water-to-binder ratio was maintained at 0.4 (with a water content of 140 kg/m^3), and 0.5% superplasticizer by weight of the binder was added to ensure adequate workability, as per the European federation for specialist construction chemicals and concrete standards. Fig. 2 illustrates the mixing procedure, along with the casting and curing process of the concrete.

Table 2. Proportions of UHPBF-HSC (Kg/m^3)

M#	Group	Code	C	CA	FA	W	BF (1.5%)	SF (10%)	SP (0.5%)	NSCBA	NCSA	NRSA
M0	REF	REF	350	1115	837	140	5.25	35	1.75	-	-	-
M1	G1 NSCBA	NSCBA1	332.5	1115	837	140	5.25	35	1.75	17.5	-	-
M2		NSCBA2	315	1115	837	140	5.25	35	1.75	35	-	-
M3		NSCBA3	397.5	1115	837	140	5.25	35	1.75	52.5	-	-
M4		NSCBA4	280	1115	837	140	5.25	35	1.75	70	-	-
M5	G2 NCSA	NCSA1	332.5	1115	837	140	5.25	35	1.75	-	17.5	-
M6		NCSA2	315	1115	837	140	5.25	35	1.75	-	35	-
M7		NCSA3	397.5	1115	837	140	5.25	35	1.75	-	52.5	-
M8		NCSA4	280	1115	837	140	5.25	35	1.75	-	70	-
M9	G3 NRSA	NRSA1	332.5	1115	837	140	5.25	35	1.75	-	-	17.5
M10		NRSA2	315	1115	837	140	5.25	35	1.75	-		35
M11		NRSA3	397.5	1115	837	140	5.25	35	1.75	-	-	52.5
M12		NRSA4	280	1115	837	140	5.25	35	1.75	-	-	70

M#-Mix number, G1-group containing nano sugar cane bagasse ash as cement replacement, G2-group containing nano cotton straw ash as cement replacement, G3-group containing nano rice straw ash as cement replacement, C-Cement, CA-Coarse aggregate, FA-Fine aggregate, W-Water, BF-Basalt fiber, SF-Silica fume, SP-Superplasticizer, NRSA-Nano rice straw ash, NSCBA-Nano sugar cane bagasse ash, NCSA-Nano cotton straw ash

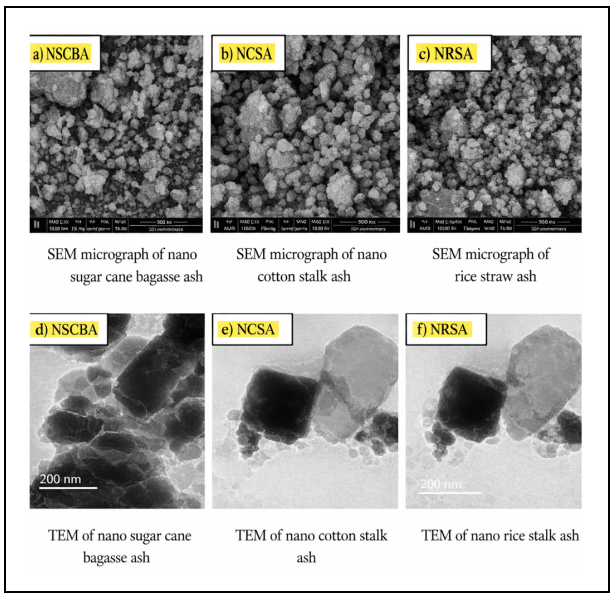


Fig. 1: Microstructures of different nanomaterials (Du *et al.* 2023)

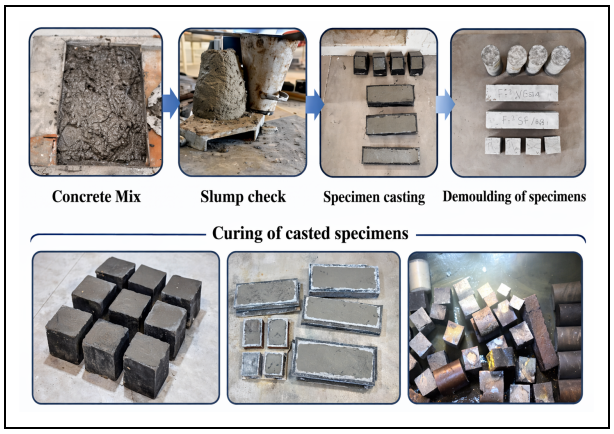


Fig. 2: Mixing, casting and curing of raw material

2.3 Furnace and Heating Rate

After 28 days of two-stage water curing, the concrete specimens were carefully removed from the curing tank and dried in an oven at 105°C for one day. This drying process aimed to reduce moisture content of the specimens, minimizing the risk of explosive spalling when exposed to high temperatures. After this, the specimens exposed to high temperatures in an electric muffle furnace to reduce any moisture related problem. Electric furnace heating was performed at a slow rate of 50°C/minute (Zeyad *et al.* 2024). A distance of about 20 mm was kept between the specimens to have a uniform thermal environment. This distance was necessary to ensure uniform heating and to avoid thermal gradients which would cause damage to the integrity of the specimens. The specimens were subjected to temperatures of 300°C and 600°C which are some of the common conditions of fire in the concrete structures. These temperatures have been selected through early experimentations and also due to the known temperatures of fire flames in high-strength concrete structures that have a range between 320°C and 400°C. This was to provide a realistic fire scenario and eliminate the possibility of explosive spalling at high-temperatures.

The furnace was heated until it attained the desired temperature and then the specimens were exposed to these conditions for one hour. This time was necessary to make sure that the specimens were subjected to the same temperature conditions so that their performance under high temperature conditions could be accurately determined. The furnace was deactivated and the specimens were left to cool slowly in the furnace after the exposure period. This cooling was done with the door of the furnace closed in order to prevent sudden changes in temperature and to avoid any thermal shock, which may affect the structural integrity of the specimens. The specimens were subjected to tests only after their temperature was ambient. All tests were conducted under stable conditions, which showed the actual effect of high temperature on the properties of the concrete.

2.4 Testing Properties and Procedures

2.4.1 Fresh Concrete Characteristics

Slump test was used to assess the workability of fresh concrete mixes as required by ASTM C143 and BS EN 12350-2. A typical slump cone with a height of 300 mm, bottom diameter of 200 mm and top diameter of 100 mm was employed. Concrete was spread into three layers, each of which was tamped with 25 blows on a tamping rod. The obtained slump values of all mixes are shown in Fig. 3. The findings show that the addition of BF and nano agricultural waste additives had an effect on the fresh state behavior of the concrete. As compared to the reference mix, slump changes were found to be different according to the type and dosage of nano material.

Even with relatively low level of water-cement ratio that characterizes high-strength concrete, all the mixes had adequate workability to be properly placed and compacted, mainly because of the application of a high-range water-reducing admixture. Testing did not show any form of segregation or bleeding, which confirms that the mixtures can be used for casting and finishing.

2.4.2 Mechanical Properties

A 3000 kN capacity digital compression testing machine was employed to evaluate the effect of nanomaterials on the mechanical properties of UHPBF-HSC. To assess compressive strength, tensile strength, and flexure strength, specimens were tested at the age of 28 days. Cube specimens (100 × 100 × 100 mm) were used for CS testing in accordance with BS EN 12390-3. Cylinder specimens (100 × 200 mm) were utilized for split tensile strength testing, following ASTM C496.

Finally, beam specimens (100 × 100 × 500 mm) were employed for flexure strength testing, adhering to ASTM C1609/C1609M.

2.4.3 Microstructure Analysis

The SEM was performed on twelve concrete mixes, four of them were representative, i.e., the reference mix M0 (REF) and three most effective mixes, i.e., M4 (NSCBA4) M7 (NCSA3) and M12 (NRSA4). These combinations were selected as the best formulations that included nano sugar cane bagasse ash, nano cotton stalk ash and nano rice straw ash, respectively. These mixes were thermally exposed to 300°C and 600°C in order to examine their effect on the microstructure due to high temperatures. The reference mix M0 was also provided in comparison. After being cured and left to dry, cube samples (10 × 10 ×10 mm) were carefully excavated out of the cores of concrete and subjected to SEM analysis. The specimens were meticulously prepared to ensure a smooth surface for imaging.

Magnification levels were varied to allow an accelerating voltage of 20 kV to produce clear and detailed microstructural images which were analyzed using the SEM. To reduce the charging effects that are normally attached to cementitious materials at high voltages, all the specimens were dried in a vacuum chamber and a thin conductive layer of gold applied before they were observed. It was a system that allowed proper analysis of crack formation, pore formation, and distribution of nano additives in the concrete base. Cracks were formed in all thermally exposed samples but significant variations in morphology and density of the cracks were noticed with the nature of nano additive added.

3. RESULTS AND DISCUSSION

3.1 Fresh Concrete Properties of UHPBF-HSC

Fig. 3 shows the slump dynamics of the reference and modified UHPBF-HSC mixtures, which make it possible to understand how nano agricultural waste additives and basalt fibers affect fresh-state performance. The reference mix (M0) showed the largest slump (88 mm) which indicated no fibers and nano-sized particles and hence increased free movement of particles and reduced internal friction in the matrix. Contrarily, all the modified mixes (M1-M12) reported lower values of slump (65 mm to 76 mm). This is largely due to the fact that nano agricultural waste materials have a high specific surface area, and thus, water adsorption is enhanced, and the quantity of free water to be lubricated is diminished.

Also, the BF are present that creates mechanical interlocking and bridging effect, which limits flow and creates greater internal resistance during deformation. Through this, the concrete is firmer and more sticky in tone. This behavior is a normal and positive trade-off of ultra-high-performance concretes, with lower slump correlated with higher packing density and greater mechanical performance.

Slump values of Group G1 (NSCBA mixes) were found to be between 68 mm and 75 mm. Such relatively increased workability of this group is explained by the finer and more homogeneous particle morphology of NSCBA, which improves the packing of the particles and decreases the excessive water demand due to the better filler and nucleation effects of the particles. Despite the fact that the decrease of the slump was lower than the reference mix (13-20 mm), the values were not out of range of placing the high-strength concrete.

The slump values of group G2 (NCSA mixes) were ranging between 65 mm to 76 mm, the lowest being of M7. It is possible that the greater reduction in slump observed in some NCSA mixes is due to the irregular particle shape and increased surface roughness of nano cotton straw ash. These characteristics enhance water absorption and increase the viscosity of the paste. This increases resistance to flow, and hence introduces increased fresh concrete behavior. Group G3 (NRSA mixes) returned 70 mm to 76 mm slump values, which means that the modified mixes had relatively good workability. This phenomenon may be attributed to the equal particle size distribution and comparatively easier surface texture of NRSA, which adds to the enhanced dispersion and decreased friction among particles and opens the opportunity to retain the flow between particles despite the fibers.

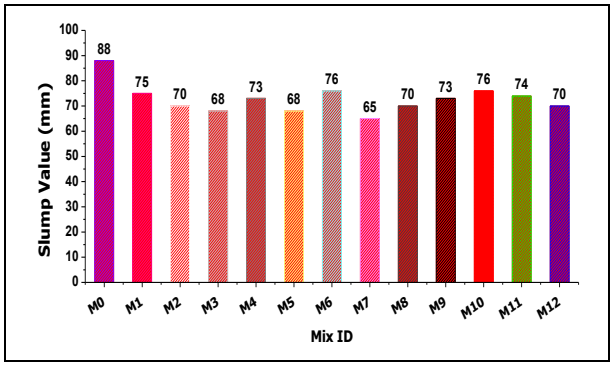


Fig. 3: Slump values for UHPBF-HSC incorporating different types of nanomaterials

In general, the range of narrow slump recorded in all of the modified mixes (65 to 76 mm) points to good homogeneity of the mix and the ability to control the rheological behavior, which supports the high efficacy of the dosage of superplasticizer in preventing excessive workability loss. Despite the observed reduction in slump in the modified mixes compared to the reference mix, the observed workability is appropriate when it comes to

UHPBF-HSC application where high fluidity is not the primary concern but rather high cohesiveness, lower segregation and elevated mechanical performance.

3.2 Hardened Concrete Properties of UHPBF-HSC

3.2.1 Water Absorption of UHPBF-HSC

Fig. 4 shows the water absorption characteristics of the concrete mixes with various nano agricultural waste additives. Water absorption of all the nano-modified concretes was greater in comparison to that of the reference mix, hence showing greater affinity to water uptake. The additives exhibited differences in water absorption with NRSA giving the best, then NCSA and NSCBA. This can be attributed to the morphology of the particles, porosity, and surface chemistry. The high specific surface area and porous structure of the nano agricultural ashes are the primary factors behind the increase in water absorption due to increased capillary suction and connectivity of the internal pores. Even though NRSA has a high content of the SiO_2, its greater water absorption is mainly explained by its finer particle size, greater specific surface area, highly porous and irregular particle morphology in contrast to NSCBA and NCSA. Burning and milling rice straw result in ash of a highly open, cellular microstructure with a high level of internal pore connectivity and thus increased capillary suction and water retention. Therefore, as observed in NRSA, physical properties like the pore structure and surface texture prevail over chemical composition, which causes increased water absorption in spite of having a large amount of silica. There is a tendency of the nano particles to absorb and hold water in the structure of these particles and with high dosage levels, the particles could also interfere with the optimum densification of the paste, provided there is also no free water to thoroughly hydrate the paste. Also, the contact between nano additives and basalt fibers can cause local modification of the pore network, which adds to an increase in the permeability pathways.

Increased water penetration is typically linked to lower resistance to corrosion, since it enables the entry of corrosive environments like chlorides and sulfates as well as exposes the product to freeze-thaw damage. This effect, however, should be combined with mechanical performance. In certain mixtures, the enhanced water absorption can be accompanied by enhanced strength as a result of augmented pozzolanic activity and polished inter-facial transition zones. In order to have a deeper insight into these conflicting effects, the water absorption findings were related to the CS, STS, and FS. Moreover, evolution of pore structure and nano-additive dispersion were analyzed by SEM technique to give microstructural evidences to support the behavior of water absorption observed.

Though nano-modified concretes have a high specific surface area and inherent porosity of nano agricultural ashes, which result in higher water absorption, there is no direct contradiction between the matrix densification. Surface-accessible and capillary pores are mostly related to increased water absorption and the pozzolanic reactions help to refine the inside of gel pore structure and the interfacial transition zones. Thus, increased water absorption in nano-modified mixes may improve the mechanical properties and localized cementitious mass densification of the cementitious matrix.

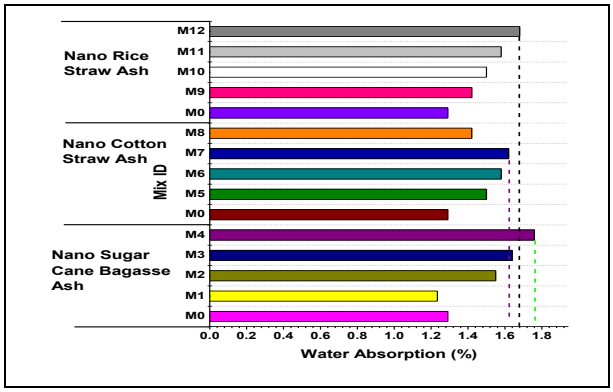


Fig. 4: Water absorption for UHPBF-HSC incorporating different types of nanomaterials

3.2.2 CS of UHPBF-HSC

The CS results in Fig. 5 are a clear indication that all mixes of concrete with NSCBA, NCSA, and NRSA along with BF, silica fume, and superplasticizer show a significant improvement in the strengths relative to the reference mix (M0). This advancement emphasizes the usefulness of nano agricultural wastes materials in improving the mechanical behavior of UHPBF-HSC. In Group G1 (NSCBA mixes), compressive strength steadily increases with NSCBA content. The highest strength was obtained with M4, 68.38 Mpa which is 47% higher than the reference mix. The high level of pozzolanic reactivity and ultra-fine particle size of NSCBA can be pointed out as the reasons of such high performance as it accelerates the secondary hydration reactions and leads to the further development of the C–S–H gel. The nano-sized particles are also micro-fillers, which have the effect of refining the pore structure and minimizing internal voids, thus, yielding a stronger and denser concrete matrix.

In Group G2 (NCSA mixes), the CS increases as compared to M0 with M7 having a peak value of 62.35 MPa representing 34% strength improvement. The NCSA-based mixes have strength enhancement which is closely related to enhanced particle packing and moderate pozzolanic activity. The relatively low reactivity of NCSA versus NSCBA does restrict the degree of strength development, however, a little,

especially at the higher replacement levels. Likewise, Group G3 (NRSA mixes) has progressive rises in strength, which means that M12 is 66.32 MPa, which is a 42.6% increase compared to the reference mix. Such enhanced performance of NRSA-based concrete can be explained by refined pore structure and increased packing density through the NRSA particles to achieve a lower level of porosity and high stress transfer in the cementitious matrix.

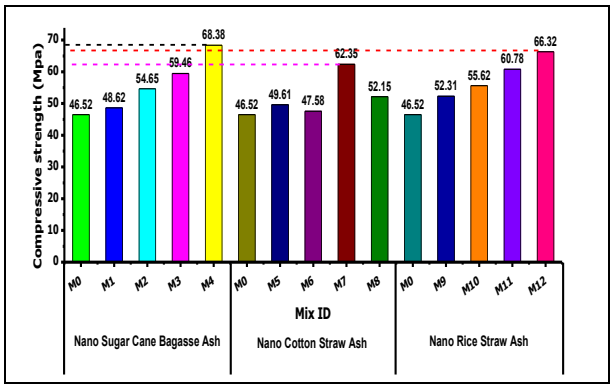


Fig. 5: CS for UHPBF-HSC incorporating different types of nanomaterials

In all groups, post-synergistic effect of nano pozzolanic materials, 1.5% BF, 10% silica fume, and 0.5% superplasticizer on the compressive strength is high. Basalt fibers are important in regulating the microcrack initiation and propagation and enhance stress redistribution during compressive loading. The silica fume also contributes to the microstructural perfection of the material filling micro-voids and increasing the speed of pozzolanic reaction, and the superplasticizer provides consistent dispersion of fibers and nano additives, resulting in sufficient workability and quality of compaction. The general findings are that the joint application of nano agricultural waste substances and BF reinforcement results in the formation of dense, crack-resistant, and high-strength UHPBF-HSC matrix. Such findings confirm the high potential of using agricultural waste in nano form to make sustainable and high-performance concrete without affecting the mechanical performance.

3.2.3 STS of UHPBF-HSC

The STS outcomes of the UHPBF-HSC blends show major improvement over the reference blend (M0) because of the addition of NSCBA, NCSA and NRSA in blend with BF. The reference mix has a baseline STS of 4.65 Mpa with all the nano-modified mixes having gradual increase with an increase in the content of nano-materials (Fig. 6), which confirms the effectiveness of the nano agricultural waste additives in improving tensile performance. A consistent rise in STS can be seen in Group G1 (NSCBA mixes) at higher levels of the NSCBA replacement level. Optimal mix, M4 (NSCBA4) has the greatest STS of 8.75 Mpa, which corresponds to 88.17% better than that of the reference mix. This dramatic improvement can be mainly explained by high pozzolanic reactivity and ultra-fine particle size of NSCBA, which enhances the creation of dense C-S-H gel and intensification of interfacial transition zone (ITZ). Polished matrix enhances the bonding between fibers and the matrix, thus, allowing BF to be effective in bridging the induced cracks and slowing down the propagation of cracks when tension is applied.

In a similar manner, Group G2 (NCSA mixes) has a significant growth in STS with M7 (NCSA3) having an STS value of 7.54 MPa, which is 62.15% higher compared to M0. Even though NCSA adds tensile strength by micro-filling and moderate pozzolanic effect, the effect of NCSA on tensile strength gain is lower than that of NSCBA because of lower reactivity of NCSA than that of NSCBA. Good particle packing and higher fiber anchorage are however of great contribution in tensile resistance. There is also an improvement with regards to progressive strength of Group G3 (NRSA mixes), where M12 (NRSA4) reached a 74.19% increase in STS compared to the reference mix. The higher performance of NRSA-based concrete can be largely related to lower porosity and transfer of stress in the matrix. It also provides a mechanism of successful load distribution between cementitious matrix and basalt fibers.

A balance nano-material dosage of 20% NSCBA (NSCBA4), 15% NCSA (NCSA3), and 20% NRSA (NRSA4) is the optimum nano-material dosage to use in each group achieving optimal STS performance. Addition of 10% silica fume brings refinement to the pore structure and improvement to the ITZ quality. Incorporation of 0.5% super plasticizer provides sufficient workability and even dispersion of the fibers and the nano additives. All these have an effect on the speed of hydration, enhance matrix cohesion and increase transfer of tensile loads.

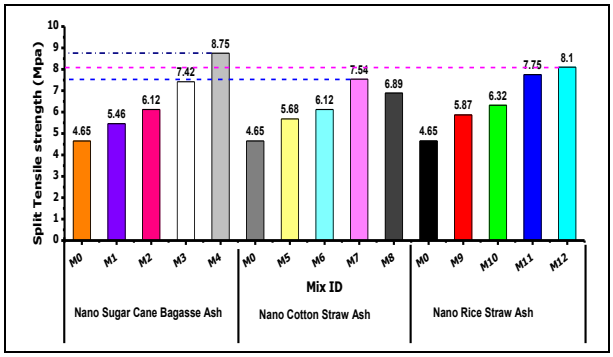


Fig. 6: STS for UHPBF-HSC incorporating different types of nanomaterials

In general, the comparison with the reference mix reveals the significance of nano agricultural waste materials and BF in enhancing the tensile performance.

NSCBA4 has the highest increase of STS, which is why it is superior to other mixes in terms of crack resistance and tensile strength improvement in UHPBF-HSC.

3.2.4 FS of UHSBF-HSC

The flexural strength performance of UHPBF-HSC mixes with NSCBA, NCSA and NRSA was compared to that of the reference mix (M0) as shown in Fig. 7. The reference mix has FS value of 5.9 MPa as the baseline whereas all nano-modified mixes have significant improvements indicating the positive effect of nano agricultural waste additives and BF on flexural behavior.

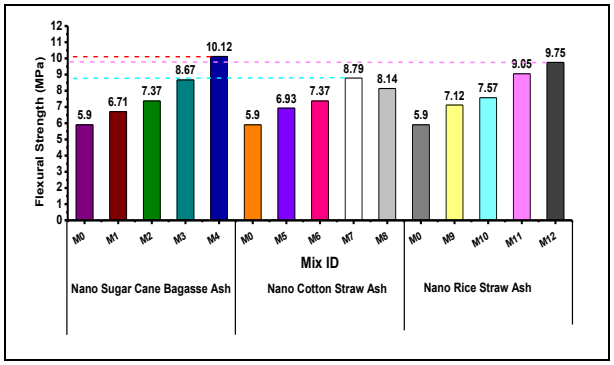


Fig. 7: FS for UHPBF-HSC incorporating different types of nanomaterials

Flexural strength in Group G1 (NSCBA mixes) also shows a positive linear increase with increment in NSCBA content, which demonstrates the significant role of NSCBA in flexural performance. The best combination, M4 (NSCBA4), has the highest FS of 10.12 Mpa, which is 71.53% higher than M0. The gradual increase of M1 to M3 (13.73, 24.92 and 46.95, respectively) indicates the increment in the degree of pozzolanic activity and filler effect of NSCBA at increased replacement levels. The nano-scaffolded NSCBA particles are efficient in refining the pore structure, make the interfacial transition zone stronger, and enhance transfer of loads between the matrix and BF under flexural loads. Group G2 (NCSA mixes) also demonstrates significant improvement in FS with M7 (NCSA3) reaching highest value of 8.79 MPa, which is a 48.98% increase compared to the reference mix. Even though the flexural gains are less than those recorded in NSCBA-based mixes, NCSA is involved in the enhanced compactness of the matrix and better anchorage of fibers, which has a positive effect on crack resistance and the flexural carrying load. In a similar manner, the Group G3 (NRSA mixes) has significant FS improvement, and M12 (NRSA4) posts a 65.25% improvement compared to M0. This enhancement in flexural performance is explained by the fact that the NRSA-based mixes have better packing of particles and fewer micro-voids that help to improve the distribution of tensile stress and slow crack initiation during the process of bending.

Highest FS performance in every group is attained at various doses of nano-materials, 20% NSCBA (M4), 15% NCSA (M7) and 20% NRSA (M12). These optimum levels indicate a pozzolanic reactivity, particle packing efficiency and fiber-matrix contact. The presence of either excessive or insufficient nano material can disrupt the continuity of the matrix or reduce hydration effectiveness. Therefore, optimum dosage levels are determined to achieve maximum flexural performance. The synergistic effect of 1.5% BF, 10% silica fume, and 0.5% super plastics is important in improving FS. Basalt fibers also bond cracks well and prevent crack propagation during bending stresses, whereas silica fume perfects the matrix and enhances the formation of C-S-H. The superplasticizer provides sufficient workability and even distribution of fibers and nano-particles, which are critical for flexural performance. In general, the interaction of nano agricultural waste materials and basalt fiber reinforcement results in a denser, tougher, and crack resistant UHPBF-HSC in comparison to the reference mix.

3.2.5 Strength Loss Due to High Temperature

Table 3 shows the effect of high temperature on compressive strength of the reference mix (M0) and the nano-modification mixes of concrete. M0 has CS 46.52 Mpa at ambient temperature (250°C) and when nano-materials are added, the CS is greatly increased. NSCBA4 (M4) has the best CS of 68.38 Mpa, then NCSA4 (M8) at 62.35 Mpa and NRSA4 (M12) at 55.62 Mpa, which means that nano-materials enhance the densification of the matrix and the initial load bearing capacity (Fig. 8). All mixes are found to have CS reduced by moisture evaporation and thermally induced microcracking when subjected to 300°C. The CS of M0 reduces to 36.29 MPa which is equivalent to approximately 22% decrease. Nevertheless, nano-modified mixes have a relatively higher strength; NSCBA4 (M4) retained 53.34 MPa which proves that nano-materials can partially overcome thermal damage by refining the pore structure and increasing the matrix cohesion. This weight loss also supports the lack of moisture and thermal effects as the main reasons of the strength reduction.

Compressive strength deteriorates at a higher rate at 600°C. The CS of M0 reduces to 26.13 Mpa, which is 43% less than that at ambient conditions. Even though NSCBA4 (M4) continues to be the strongest nano-modified mix with a strength of 38.40 Mpa a significant drop can be seen in the strength as a result of excessive dehydration, thermal expansion incompatibility and decomposition of hydration products. These findings show that NSCBA, NCSA, and NRSA increase thermal resistance than the reference mix but their performance decreases at high temperatures. In general, the results prove that nano-materials enhance residual CS with

moderate temperature exposure, yet severe strength decline is inevitable at high temperatures, which necessitates additional adjustment of concrete mixes to extreme temperatures.

Table 3. Strength properties at various temperatures

M#	Group	Code	Temp 25°C	Temp 300°C			Temp 600°C		
			CS, MPa	CS, MPa	% Reduction Strength	Weight Loss	CS, MPa	% Reduction Strength	Weight Loss
M0	REF	REF	46.52	36.29	-0.22	0.056	26.13	-0.43	0.15
M1	G1 NSCBA	NSCBA1	48.62	38.92	-0.19	0.048	28.30	-0.41	0.12
M2		NSCBA2	54.65	42.53	-0.22	0.063	31.69	-0.42	0.16
M3		NSCBA3	59.46	47.38	-0.20	0.055	34.39	-0.42	0.15
M4		NSCBA4	68.38	53.34	-0.22	0.061	38.40	-0.43	0.17
M5	G2 NCSA	NCSA1	46.52	36.29	-0.22	0.048	26.13	-0.43	0.14
M6		NCSA2	49.61	39.70	-0.19	0.054	27.86	-0.43	0.15
M7		NCSA3	47.58	37.11	-0.22	0.062	29.72	-0.37	0.16
M8		NCSA4	62.35	47.63	-0.23	0.056	35.02	-0.43	0.13
M9	G3 NRSA	NRSA1	52.15	41.68	-0.20	0.063	31.29	-0.40	0.15
M10		NRSA2	48.52	36.29	-0.22	0.059	26.13	-0.43	0.12
M11		NRSA3	52.31	42.80	-0.18	0.048	29.38	-0.43	0.12
M12		NRSA4	55.62	44.38	-0.20	0.053	32.24	-0.42	0.15

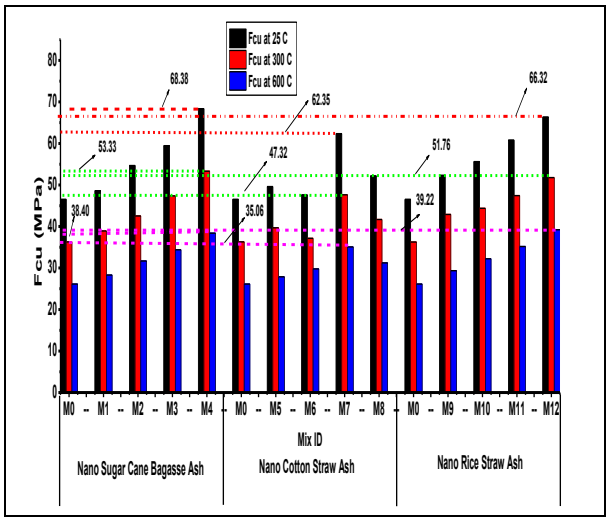


Fig. 8: CS for UHPBF-HSC incorporating different types of nanomaterials under elevated temperatures

3.2.6 Mass Loss Due to Temperature

Weight loss can serve as an indicator of calcium silicate hydrate (CSH) and calcium hydroxide (CH) decomposition in concrete exposed to elevated temperatures. All specimens were initially weighed under ambient conditions and subsequently subjected to thermal treatment in a muffle furnace for 2 hours at the desired temperature. The nano-enhanced concrete mixes showed a small mass loss of 2.7-4.5%, which was significantly lower compared to the 5.3% mass loss that was seen in the control mix. This minimization of mass can be explained by the fact that in nano-enhanced mixes there are increased pozzolanic reactions and more compact microstructures, which create fewer pores. Exception was however observed in mixes with NSCBA that showed loss of mass by 7.3%, which is attributed to lower filler content. Although the mass loss in nano-enhanced concretes was small, great decrease in strength was observed at high temperatures. Such difference can be explained by the decomposition of CH, which is one of the main components that makes concrete strong. Higher temperature treatment led to increased ratio of mass loss up to 11.6 to 14.5 % in nano mixes which further justified the decomposition of CH (Mostafa *et al.* 2022).

3.2.7 Ultrasonic Pulse Velocity for UHPBF-HSC Incorporating Different Types of Nanomaterials

The results of the Ultrasonic Pulse Velocity (UPV) of all concrete mixes are presented in Fig. 9. The mixes show high quality concrete based on the measurements of the UPV. It is worth noting that concrete that contained 20% of NSCBA4 (M4) had better velocity than the control mix (M0). On the same note, the blend with 20% NRSA4 (M12) too exhibited improved velocity. On the contrary, the mixture consisting of 5% NCSA1 recorded the highest velocity in its group, as it has a high surface area. In G1, the UPV results follow the order: NSCBA4 (M4) > NSCBA3 (M3) > NSCBA2 (M2) > NSCBA1 (M1) > REF (control). This series shows that the increase in nano sugarcane bagasse ash content usually leads to improved quality of concrete with NSCBA4 offering the best velocity. In G2 with nano cotton straw ash, the UPV order is: NCSA1 (M5) > NCSA2 (M6) > NCSA4 (M8) > NCSA3 (M7) > REF (control). Here, 5% NCSA1 achieved the highest velocity. For Group 3, which includes nano rice straw ash, the UPV results are: NRSA4 (M12) > NRSA3 (M11)

> NRSA1 (M9) > NRSA2 (M10) > REF (control). In this group, 20% NRSA4 exhibited the best velocity.

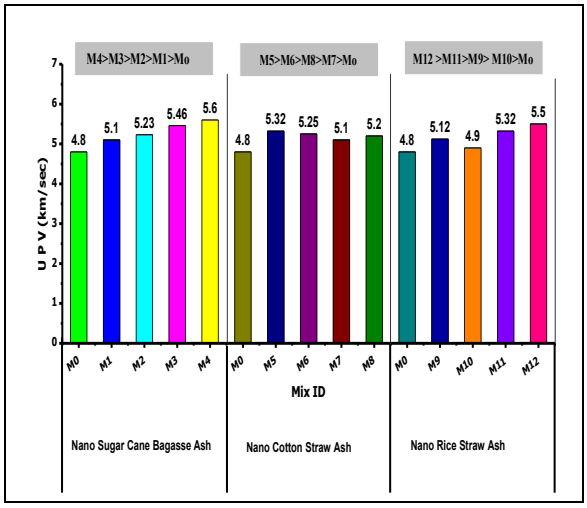


Fig. 9: UPV for UHPBF-HSC incorporating different types of nanomaterials

At the bottom (M0), the UPV is 4.8 km/s. The addition of nano-material and BF tend to maximize the UPV values indicating the enhancement of the concrete density and the internal structure. The values of UPSV are found to increase with the percentage of nano sugar cane bagasse ash in G1. An example is NSCBA1 (M1): with an increase of 6.25% over the M0, the UPV of 5.1 km/s. This trend continues with NSCBA2 (M2) at 5.23 km/s, NSCBA3 (M3) at 5.46 km/s, and the highest at NSCBA4 (M4) with 5.6 km/s, marking a significant 16.67% increase. The increased values of UPV show that an increase in the NSCBA content increases the density of the concrete and its internal bonding. The values of UPV in group G2 (NCSA) have moderate growth relative to M0. NCSA1 (M5) achieves a UPV of 5.32 km/s, a 10.42% increase, while NCSA2 (M6) has a slight decrease to 5.25 km/s. NCSA3 (M7) and NCSA4 (M8) exhibit UPV values of 5.1 km/s and 5.2 km/s, respectively, with increases of 6.25% and 8.33% compared to M0. This indicates that while the addition of NCSA generally improves UPV, the effect is less pronounced compared to NSCBA. Group G3 (NRSA) shows a similar trend with NRSA materials. NRSA1 (M9) has a UPV of 5.12 km/s, a 6.67% increase over M0, while NRSA2 (M10) shows a decrease to 4.9 km/s. NRSA3 (M11) and NRSA4 (M12) achieve UPV values of 5.32 km/s and 5.5 km/s, respectively, marking increases of 10.42% and 14.58% compared to M0. The optimum mix in this group is NRSA4 (M12) with a UPV of 5.5 km/s, indicating the most significant improvement in density and internal structure.

In general, the results of the UPV produced a high correlation with CS, STS, and FS. The increased values in the UPV means there is an increase in the microstructure, less microcracking, and an enhanced transmission of stress waves. The effects of nano-materials, basalt fibers, silica fume, and superplasticizer, are synergistic, which makes UHPBF-HSC have a better internal structure and durability. Of all the mixes, NSCBA4 and NRSA4 depict the greatest enhancements in UPV, attesting to their efficiency in generating the high quality and strength concrete, whereas NCSA demonstrates the best performance at reduced levels of replacement.

The ASTM C597 classification criteria state that the higher the value of the UPV, the higher the quality of concrete with a high density and low internal defects. The reference mix (M0) in the current study had a UPV of 4.8 km/s and therefore this material is excellent-quality concrete. The UHPBF-HSC mixes with nano-modifications displayed values of UPV in the range of 4.9 to 5.6 km/s. Uniformly high UPV values are an affirmation of the high density of the microstructure, enhanced internal bonding, and lower microcracking of the composite through the use of nano agricultural waste materials, BF, silica fume, and superplasticizer. The identified classification also justifies the recorded increases in compressive, tensile and flexural strengths.

3.2.8 Comparison with Standard Acceptance Criteria

The values of the UPV of all mixes are in the range of international standards of good-quality concrete. In reference to the standards of IS 13311 (Part 1): 1992, ASTM C597 and BS EN 12504-4, having a higher value of UPV than 4.5 km/s is a sign of excellent concrete with a high density and minimal internal defects. All the mixes, such as the reference mix (M0) with the UPV of 4.8 km/s, and the nano-modified mixes, such as NSCBA4 (5.6 km/s) and NRSA4 (5.5 km/s), meet this requirement in the current study, but considerably surpass the threshold indicating the enhanced internal compactness, decreased microcracking, and stress-wave transmission.

In the case of water absorption, standards like ASTM C642 and IS 3085 do not mandate a specific maximum level of water absorption, but the values of the water absorption less than 5-6% are generally reasonable for structural use and permanent performance. The perceived increase in the absorption of water by nano-modified concretes is agreeable to acceptable levels in the literature on high-performance and nano-modified cementitious composites. It is mainly related to surface-accessible pores and high specific surface area of nano agricultural ashes. Concomitantly, internal matrix densification by pozzolanic reactions is also verified by better CS, STS, FS, and UPV values.

The overall assessment of UPV, mechanical strength, and water absorption, therefore, indicates that all UHPBF-HSC mixes meet the standard quality criteria and have a higher structural integrity with a localized enhancement in water uptake.

3.3 Microstructure Analysis for UHPBF-HSC

3.3.1 SEM Analysis for UHPBF-HSC Used with and without Nanomaterials at 25℃

Fig. 10 presents the SEM micrographs for four distinct mixes of M0 (reference), M4 (NSCBA4), M7 (NCSA3), and M12 (NRSA4) at ambient temperature. These mixes were selected based on their mechanical performance, reflecting the optimum strength achieved. The images reveal a tightly bonded matrix, showing robust interactions between the matrix components and the added fibers. The use of nanoparticles enhances the sustained development of CSH gel, which helps to transform the CH crystals and hasten the hydration process. It leads to the improved microstructure through which the presence of amorphous silica caused by the nanoparticles increases the strength of the gel more efficiently than CH crystals, and the interfacial transition zone (ITZ) performance (Yonggui *et al.* 2020).

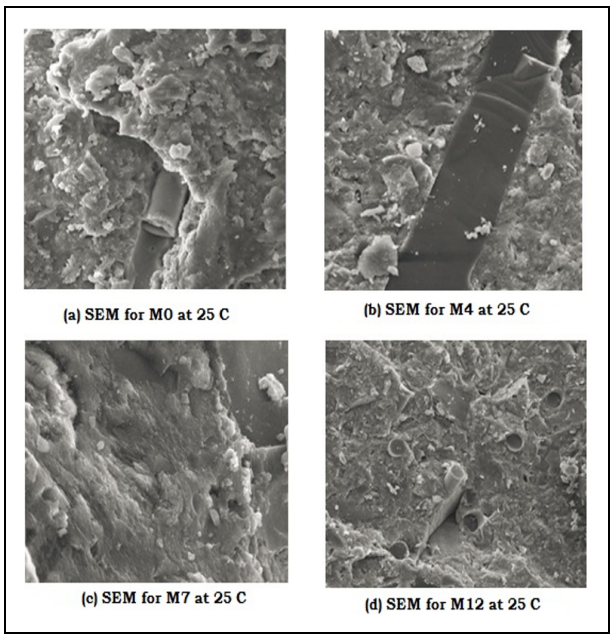


Fig. 10: SEM for UHPBF-HSC used with and without nano materials at 25℃

3.3.2 SEM Analysis for UHPBF-HSC Used with and Without Nanomaterials at 300℃

The elevated temperature (300°C) creates an effect of massive alterations in the mixes (M0, M4, M7, and M12) composition. The internal damage is observed in all samples because of the processes of ettringite decomposition and water evaporation resulting in microcracks (Fig. 11). Microcrack propagation and stress concentration is also found at high temperatures especially in highly compacted mixtures containing ultra-fine materials. Loss of adsorbed and capillary water leads to the increased porosity and the change in material structure (Yonggui *et al.* 2020).

3.3.3 SEM Analysis for UHPBF-HSC Used with and without nanomaterials at 600℃

Fig. 12 shows the SEM micrographs for concrete mixes M0, M4, M7, and M12 at 600°C. At this temperature, random cracking is widespread across all mixes. This phenomenon is attributed to the complete decomposition of ettringite and CH crystals, which disrupts the CSH hydration products. The reaction weakens the ITZ between the gel and the surrounding matrix, creating weak zones that may coalesce. Additionally, the high temperature exacerbates pore formation, with small voids generated at lower temperatures increasing in size due to further water evaporation and structural degradation (Yonggui *et al.* 2020).

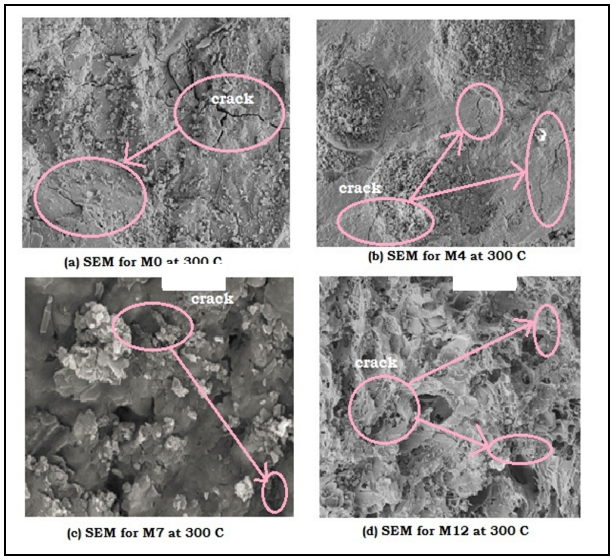


Fig. 11: SEM for UHPBF-HSC used with and without nano materials at 300℃

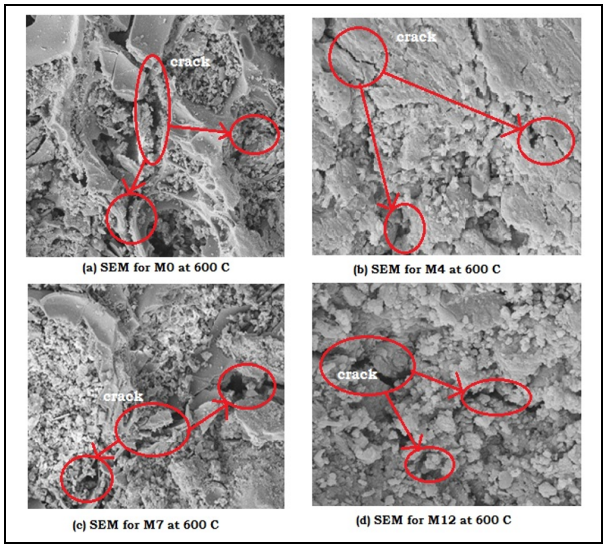


Fig. 12: SEM for UHPBF-HSC used with and without nano materials at 600℃

3.4 Comparison and Predicted STS and FS from Literature

The empirical formulations used in estimation of the STS and FS of concrete are listed in Table 4 based on the literature. Table 5 and Table 6 give comparative analysis of the STS and FS values experimentally measured and coded, predicted using different international standards and published models of the various concrete mixes. The reference mix (M0) shows an experimental STS value of 46.52 MPa, which exceeds predictions from references (Chen *et al.* 1980; Carino *et al.* 1982; Oluokun *et al.* 1991; which estimate 4.65 MPa, 5.72 MPa, and 4.16 MPa, respectively. This discrepancy suggests that current models may underestimate the tensile strength of the reference mix. Incorporating NSCBA significantly enhances STS. For example, NSCBA4 (M4) achieves an experimental STS of 8.75 MPa (Fig. 13), surpassing the predictions from references (An *et al.* 2025; Almohammed *et al.* 2024; Saha *et al.* 2024), which range from 5.09 MPa to 5.68 MPa. Similarly, NCSA improves STS, with NCSA4 (M8) reaching 6.89 MPa, but predictions from codes (An *et al.* 2025; Almohammed *et al.* 2024; Saha *et al.* 2024) ranging from 4.78 MPa to 5.38 MPa, are lower. NRSA also shows competitive performance, with NRSA4 (M12) recording 8.1 MPa, exceeding predictions from references (Chen *et al.* 1980; Carino *et al.* 1982; Oluokun *et al.* 1999), which are between 4.43 MPa and 5.03 MPa. Fig. 14 shows the results of multiple regression analysis for predicted STS values.

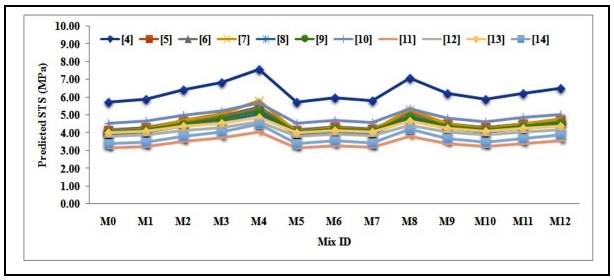


Fig. 13: Comparison graph for exp. value (CS) and predicted STS values for various codes and reference

Regarding FS, the experimental value for M0 is 5.9 MPa, while predictions from references (Ahmed *et al.* 2008; Legeron *et al.* 2000; Eme *et al.* 2019) range from 2.05 MPa to 4.74 MPa, indicating that standard models may not fully capture the flexural performance of the reference mix. For NSCBA mixes, FS values are notably higher than predicted, with NSCBA4 (M4) showing an experimental FS of 10.1 MPa, whereas predictions from references (Khan *et al.* 2024; ACI 363, 1997; ACI 318, 1999) range from 5.13 MPa to 7.78 MPa. NCSA mixes also demonstrate increased FS, with NCSA4 (M8) achieving 8.14 MPa, surpassing predictions from codes (ACI 363, 1997; ACI 318, 1999), which are between 4.90 MPa and 6.40 MPa. NRSA mixes, particularly NRSA4 (M12) with 9.75 MPa (Fig. 15), exceed predictions from earlier references (Ahmed *et al.* 2008; Legeron *et al.* 2000; Eme *et al.* 2019), which range from 2.24 MPa to 5.97 MPa. This shows better performance by NRSA in increasing FS over the traditional models. Fig. 16 shows multiple regression analysis for predicted FS values.

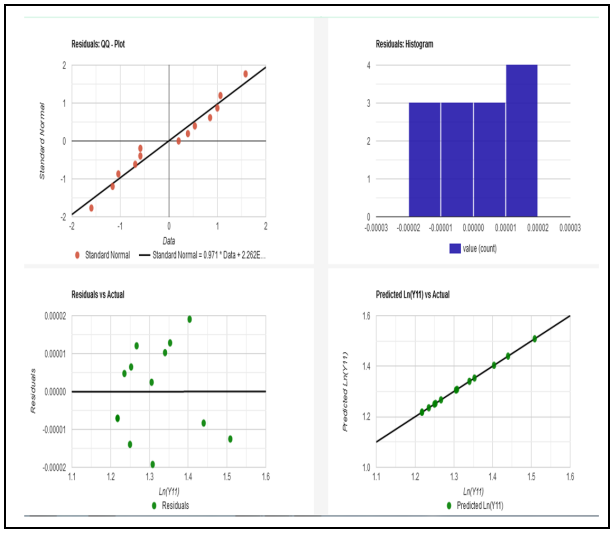


Fig. 14: Multiple regression analysis for predicted STS values from literature

Table 4. Formula used for the predicted values of STS and FS of UHPBF-HSC

Author	Formula	ID
Formula for predicted STS values of UHPBF-HSC		
Chen *et al.* 1980	$f_{sp} = 0.34\ f_C^{0.735}$	4
(Carino *et al.* 1982)	$f_{sp} = 0.272\ f_C^{0.71}$	5
(Oluokun *et al.* 1991)	$f_{sp} = 0.294\ f_C^{0.69}$	6
(Khan *et al.* 2024)	$f_{sp} = 0.106\ f_C^{0.948}$	7
(An *et al.* 2025)	$f_{sp} = 0.3\ f_C^{2/3}$	8
(Almohammed *et al.* 2024)	$f_{sp} = 0.313\ f_C^{0.667}$	9
(Saha *et al.* 2024)	$f_{sp} = 0.47\ f_C^{0.59}$	10
(El *et al.* 2025)	$f_{sp} = 0.301\times(0.8\times f_{ck})^{0.65}$	11
(ACI 363, 1997)	$f_{sp} = 0.56 f_C^{0.5}$	12
(ACI 318, 1999)	$f_{SP} = 0.59\ \sqrt{f}$	13
(GB 50010-2010, 2015)	$f_{sp} = 0.19\times(f_{ck})^{0.75}$	14
Formula for predicted FS values of UHPBF-HSC		
(Ahmed *et al.* 2008)	$f_b = 0.3 f_c^{0.5}$	1
(Legeron *et al.* 2000)	$f_b = 0.68\ f_c^{0.5}$	2
(Eme *et al.* 2019)	$f_b = 0.23 f_c^{0.75}$	3
(Khan *et al.* 2024)	$f_b = 0.034 f_c^{1.286}$	7
(ACI 363, 1997)	$f_b = 0.62\times(f_{ck})^{0.5}$	12
(ACI 318, 1999)	$f_b = 0{:}94 f_c^{0.5}$	13
CEB-FIP 2010	$f_b = 0.81\times(f_{ck})^{0.5}$	14
(IS 456-2000)	$f_b = 0.70\times(f_{ck})^{0.5}$	15

Table 5. Comparison and predicted STS values from various codes and references

M#	Group	Code	Experimental Values (MPa)		ID										
			F_c	f_{sp}	4	5	6	7	8	9	10	11	12	13	14
M0	REF	REF	46.52	4.65	5.72	4.16	4.16	4.04	3.93	4.05	4.53	3.16	3.82	4.02	3.38
M1	G1 NSCBA	NSCBA1	48.62	5.46	5.91	4.29	4.29	4.21	4.05	4.17	4.65	3.25	3.90	4.11	3.50
M2		NSCBA2	54.65	6.12	6.44	4.66	4.65	4.70	4.38	4.51	4.98	3.51	4.14	4.36	3.82
M3		NSCBA3	59.46	7.42	6.85	4.95	4.93	5.10	4.63	4.77	5.23	3.71	4.32	4.55	4.07
M4		NSCBA4	68.38	8.75	7.59	5.46	5.43	5.82	5.09	5.24	5.68	4.06	4.63	4.88	4.52
M5	G2 NCSA	NCSA1	46.52	5.68	5.72	4.16	4.16	4.04	3.93	4.05	4.53	3.16	3.82	4.02	3.38
M6		NCSA2	49.61	6.12	5.99	4.35	4.35	4.29	4.10	4.23	4.70	3.29	3.94	4.16	3.55
M7		NCSA3	47.58	7.54	5.81	4.22	4.22	4.13	3.99	4.12	4.59	3.21	3.86	4.07	3.44
M8		NCSA4	62.35	6.89	7.09	5.12	5.09	5.33	4.78	4.93	5.38	3.82	4.42	4.66	4.22
M9	G3 NRSA	NRSA1	52.15	5.87	6.22	4.51	4.50	4.50	4.24	4.37	4.84	3.40	4.04	4.26	3.69
M10		NRSA2	48.52	6.32	5.90	4.28	4.28	4.20	4.04	4.17	4.64	3.25	3.90	4.11	3.49
M11		NRSA3	52.31	7.75	6.23	4.52	4.51	4.51	4.25	4.38	4.85	3.41	4.05	4.27	3.70
M12		NRSA4	55.62	8.1	6.52	4.72	4.70	4.78	4.43	4.57	5.03	3.55	4.18	4.40	3.87

Table 6. Comparison and predicted FS values from various codes and references

M#	Group	Code	Experimental Values (MPa)		ID							
			F_c	F_b	1	2	3	7	12	13	14	15
M0	REF	REF	46.52	5.9	2.05	4.64	4.10	4.74	4.23	6.41	5.52	4.77
M1	G1 NSCBA	NSCBA1	48.62	6.71	2.09	4.74	4.23	5.02	4.32	6.55	5.65	4.88
M2		NSCBA2	54.65	7.37	2.22	5.03	4.62	5.83	4.58	6.95	5.99	5.17
M3		NSCBA3	59.46	8.67	2.31	5.24	4.92	6.50	4.78	7.25	6.25	5.40
M4		NSCBA4	68.38	10.1	2.48	5.62	5.47	7.78	5.13	7.77	6.70	5.79
M5	G2 NCSA	NCSA1	46.52	6.93	2.05	4.64	4.10	4.74	4.23	6.41	5.52	4.77
M6		NCSA2	49.61	7.37	2.11	4.79	4.30	5.15	4.37	6.62	5.71	4.93
M7		NCSA3	47.58	8.79	2.07	4.69	4.17	4.88	4.28	6.48	5.59	4.83
M8		NCSA4	62.35	8.14	2.37	5.37	5.10	6.91	4.90	7.42	6.40	5.53
M9	G3 NRSA	NRSA1	52.15	7.12	2.17	4.91	4.46	5.49	4.48	6.79	5.85	5.06
M10		NRSA2	48.52	7.57	2.09	4.74	4.23	5.01	4.32	6.55	5.64	4.88
M11		NRSA3	52.31	9.05	2.17	4.92	4.47	5.52	4.48	6.80	5.86	5.06
M12		NRSA4	55.62	9.75	2.24	5.07	4.68	5.97	4.62	7.01	6.04	5.22

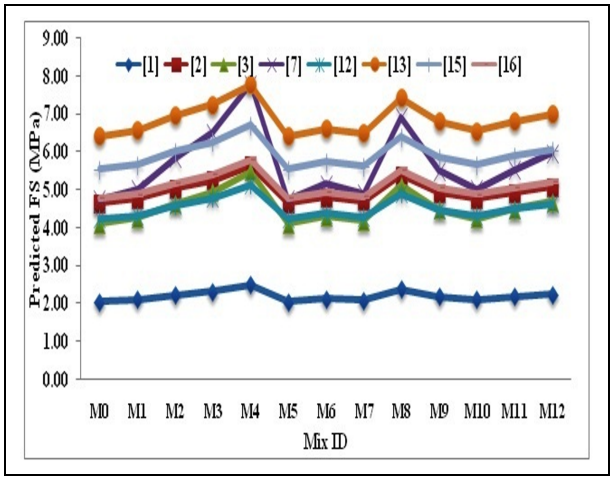


Fig.15: Comparison graph for exp. value (CS) and predicted FS values for various codes and reference

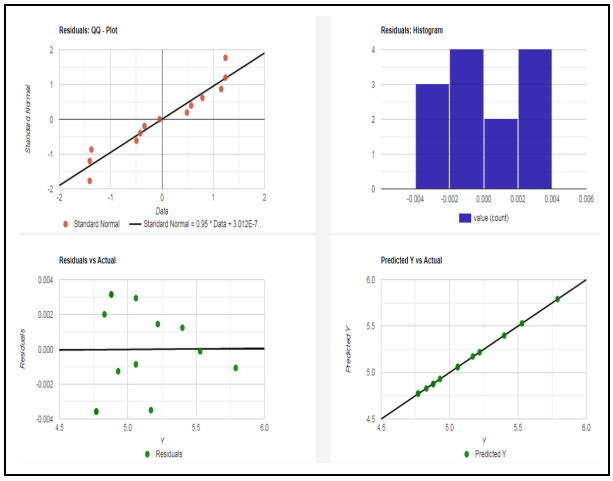


Fig. 16: Multiple regression analysis for predicted FS values from literature

4. CONCLUSION

The study demonstrates that incorporating nano agricultural waste materials (NSCBA, NCSA, and NRSA), silica fume, and basalt fibers significantly improves the performance of UHPBF-HSC. Nano additives enhance compressive, split tensile, and flexural strengths, with the best results observed in mixes containing nano sugarcane bagasse ash. The optimum NSCBA mix achieved a 47% increase in compressive strength, an 88.17% improvement in split tensile strength, and up to a 71.53% increase in flexural strength compared with the reference mix. Basalt fibers further improved tensile resistance and crack control, while UPV results confirmed better matrix density and internal quality. Although compressive strength decreased at elevated temperatures (300 ℃ and 600 ℃), nano-enhanced mixes still exhibited superior performance compared with the control mix. These results highlight the strong potential of nano agricultural waste and basalt fibers for producing high-performance, durable, and sustainable concrete suitable for structural applications.

FUNDING

This research received no specific grant from any funding agency in the public, commercial, or not-for-profit sectors.

CONFLICTS OF INTEREST

The authors declare that there is no conflict of interest.

COPYRIGHT

This article is an open-access article distributed under the terms and conditions of the Creative Commons Attribution (CC BY) license (http://creativecommons.org/licenses/by/4.0/).

REFERENCES

Abbas, A. A. H., Kharun, M. and Chiadighikaobi, P. C., The effect of minibars basalt fiber fraction on mechanical properties of high-performance concrete, *Cogent Eng.*, 9(1), 2136603(2022). https://doi.org/10.1080/23311916.2022.2136603

Abid, M., Waqar, G. Q., Mao, J., Javed, M. F. and Almujibah, H., Mechanical properties, microstructure and GEP-based modeling of basalt fiber reinforced lightweight high-strength concrete containing SCMs, *J. Build. Eng.*, 96, 110378(2024). https://doi.org/10.1016/j.jobe.2024.110378

ACI Committee 318, Building Code Requirements for Structural Concrete (ACI 318-99) and Commentary, 318R-99, American Concrete Institute, Farmington Hills (1999). https://ia600409.us.archive.org/26/items/1.ACI31899/1.%20ACI%20-318-99.pdf

ACI Committee 363, State-of-the-Art Report on Highstrength Concrete, ACI 363R-92, American Concrete Institute, Farmington Hills (1997). https://www.silicafume.org/pdf/reprints-363rtoc.pdf

Ahmed, M., Dad, K. M. K. and Wamiq, M., Effect of concrete cracking on the lateral response of RCC buildings, *Asian J. Civ. Eng. Build. Housing*, 9 (1), 25e34(2008).

Almohammed, F., Thakur, M. S., Lee, D., Kumar, R. and Singh, T., Flexural and split tensile strength of concrete with basalt fiber: An experimental and computational analysis, *Construct. Build. Mater.*, 414, 134936(2024). https://doi.org/10.1016/j.conbuildmat.2024.134936

Alomayri, T. and Ali, B., Effect of plant fiber type and content on the strength and durability performance of high-strength concrete, *Constr. Build. Mater.*, 394, 132166(2023). https://doi.org/10.1016/j.conbuildmat.2023.132166

Althoey, F., Zaid, O., Alsulamy, S., Martínez-García, R., de Prado-Gil, J. and Arbili, M. M., Experimental study on the properties of ultra-high-strength geopolymer concrete with polypropylene fibers and nano-silica, *Plos one*, 18(4), e0282435(2023). https://doi.org/10.1371/journal.pone.0282435

Amin, M., Zeyad, A. M., Tayeh, B. A. and Agwa, I. S., Effects of nano cotton stalk and palm leaf ashes on ultrahigh-performance concrete properties incorporating recycled concrete aggregates, *Constr. Build. Mater.*, 302, 124196(2021). https://doi.org/10.1016/j.conbuildmat.2021.124196

An, F. C., The Effects of Different Constitutive Compression Models of Concrete on the FRP–Concrete Bonded Interface, *Int. J. Polym. Sci.*, 2025(1), 7722361(2025). https://doi.org/10.1155/ijps/7722361

Anish, V. and Logeshwari, J., A review on ultra-high-performancefibre-reinforced concrete with nanomaterials and its applications, *J. Eng. Appl. Sci.*, 71(1), 25(2024). https://doi.org/10.1186/s44147-023-00357-8

Batool, F., Masood, A. and Ali, M., Characterization of sugarcane bagasse ash as pozzolan and influence on concrete properties, *Arab. J. Sci. Eng.,* 45(5), 3891-3900(2020). https://doi.org/10.1007/s13369-019-04301-y

Berktaş, İlayda., Facile synthesis of graphite-and graphene-based hybrid additives by silanization and effects of these additives on the thermal conductivity of cementitious grouts used in shallow geothermal systems, *PhD diss.,* (2020). https://research.sabanciuniv.edu/id/eprint/41491

Carino, N. J. and Lew, H. S., Re-examination of the relation between splitting tensile and compressive strength of normal weight concrete, *ACI J. Proce.,* 79 (3), 214e219(1982). https://doi.org/10.14359/10900

Chen, W. F. and Robert, L. Y., Tensile strength of concrete: Double-punch test., *J. Struc. Division,* 106 (8), 1673-1693(1980). https://doi.org/10.1061/JSDEAG.0005493

Du Beton, C. E. I., CEB-FIP Model Code 2010; CEB-FIP: Lausanne, Switzerland, (2012). https://site.abece.com.br/wp-content/uploads/2023/09/fib_Bull65_NMG.pdf

Du, B., Xu, F., AlAteah, A. H. and Mostafa, S. A., Sustainable development of ultra high-performance concrete using basil plant waste: Investigation at normal and extreme conditions, *J. Build. Eng.*, 80, 107997(2023). https://doi.org/10.1016/j.jobe.2023.107997

El Berdai, Y., Taha, Y., Safhi, A. M., Trauchessec, R., Hakkou, R. and Benzaazoua, M., How Does Coarse Aggregate Type Influence Mechanical Properties of High-Strength Concrete?, *ACI Mater. J.*, 122(3), 79-87(2025). https://doi.org/10.14359/51746716

Eme, D. B. and Nwaobakata, C., Effect of water cement ratio variation and coarse aggregate gradation on the compressive strength of cement concrete, *Int. Res. J. Adv. Eng. Sci.*, 4(1), 115-122(2019). http://irjaes.com/wp-content/uploads/2020/10/IRJAES-V4N1P57Y18.pdf

GB 50010-2010; Chinese Standard Code for Design of Concrete Structures, MOHURD: Beijing, China, (2015). https://doi.org/10.1155/ijps/7722361

Huang, K., Xie, J., Wang, R., Feng, Y. and Rao, R., Effects of the combined usage of nanomaterials and steel fibres on the workability, compressive strength, and microstructure of ultra-high-performance concrete, *Nanotechnol. Rev.*, 10(1), 304-317(2021). https://doi.org/10.1515/ntrev-2021-0029

Hussain, L. N., Hamood, M. J. and Al-Shaarbaf, E. A., Behavior of ultra-high-performance concrete deep beams reinforced by basalt fibers, *Open Eng.*, 14(1), 20240019 (2024). https://doi.org/10.1515/eng-2024-0019

IS – 456: 2000; Plain Concrete and Reinforced, Bureau of Indian Standards: New Delhi, India, (2000). https://law.resource.org/pub/in/bis/S03/is.456.2000.pdf

Khan, M. M. and Iqbal, M. A., Strain rate and size effects on dynamic tensile behaviour of standard and high-strength concrete: an experimental study, *Struc.,* 63, 106325(2024). https://doi.org/10.1016/j.istruc.2024.106325

Legeron, F. and Paultre, P., Prediction of modulus of rupture of concrete, ACI Mater. J. 97 (2), 193e200(2000). https://doi.org/10.14359/823

Mostafa, S. A., Bassam A. T. and Ibrahim, A., Investigation the properties of sustainable ultra-high-performance basalt fibre self-compacting concrete incorporating nano agricultural waste under normal and elevated temperatures, *Case Stud. Constr. Mater.,* 17, e01453(2022). https://doi.org/10.1016/j.cscm.2022.e01453

Muniyasamy, M. K. and Dinesh, K. M., Analyzing the Characteristics of Self-Compacting, Basalt Fiber, Ultra-High-Performance Concrete Using Nanowaste Product at Both High and Normal Temperature Changes, *Int. Conf. Civ. Eng. Innov. Develop. Eng. Adv.,* 387, 21-30(2023). https://doi.org/10.1007/978-981-99-6175-7_3

Nasser, I. M., Ibrahim, M. H. W., Zuki, S. S. M., Algaifi, H. A. and Alshalif, A. F., The effect of nanosilica incorporation on the mechanical properties of concrete exposed to elevated temperature: a review, *Environ. Sci. Pollut. Res.*, 29(11), 15318-15336(2022). https://doi.org/10.1007/s11356-021-18310-8

Oluokun, F. A., Burdette, E. G. and Deatherage, J. H., Splitting tensile strength and compressive strength relationships at early ages, *ACI Mater. J.,* 88 (2), 115-121(1991). https://doi.org/10.14359/1859

Perera, M. A. G. P. and Ranjith, P. G., Eco-friendly cementitious composites for enhanced strength: Emerging trends and innovations, *J. Clean. Prod.*, 468, 142962(2024). https://doi.org/10.1016/j.jclepro.2024.142962

Saha, A., Tonmoy, T. M., Sobuz, M. H. R., Aditto, F. S. and Mansour, W., Assessment of mechanical, durability and microstructural performance of sulphate-resisting cement concrete over portland cement in the presence of salinity, *Constr. Build. Mater.*, 420, 135527(2024). https://doi.org/10.1016/j.conbuildmat.2024.135527

Shi, C., Wu, Z. and Banthia, N., Ultra-high-performance concrete, *Des. Perf. appli.*, 504(2024). https://doi.org/10.1201/9781003203605

Sun, T., Wang, X., Ashour, A. and Han, B., 16-Sustainable ultra-high-performance concrete materials and structures, *Sustain. Concre. Mater. Struct.,* 487-529(2024). https://doi.org/10.1016/B978-0-443-15672-4.00016-4

Supit, S. W., Nishiwaki, T., Shaikh, F. U., Boonserm, K. and Rahman, S. A., Influences of hybrid fiber-reinforcement using wollastonite and cellulose nanofibers on strength and microstructure characterization of ultra-high-performance mortar, *Constr. Build. Mater.*, 423, 135802(2024). https://doi.org/10.1016/j.conbuildmat.2024.135802

Tran, H. B., Le, V. B. and Phan, V. T. A., Mechanical properties of high strength concrete containing nano SiO_2 made from rice husk ash in southern Vietnam, *Cryst.*, 11(8), 932(2021). https://doi.org/10.3390/cryst11080932

Ubayi, S. M., Mathur, C. V., Abubakar, B. S. and Idris, H. I., Rice Husk Ash in Concrete: A Review of Cement Replacement Proportions and Mechanical Properties, *Int. J. Eng. Sci*., 1(5), 1-15(2024). https://doi.org/10.5281/zenodo.13888854

Ünal, M. T., Hashim, H. B., Gökçe, H. S., Ayough, P., Köksal, F., El-Shafie, A., Osman, S. and Pordesari, A., Development and Characterization of Basalt Fiber-Reinforced Green Concrete Utilizing Coconut Shell Aggregates, *Sustain.*, 16(17), 7306(2024). https://doi.org/10.3390/su16177306

Ünal, M. T., Gökçe, H. S., Ayough, P., Alnahhal, A. M., Şimşek, O. S. M. A. N. and Nehdi, M. L., Nanomaterial and fiber-reinforced sustainable geopolymers: A systematic critical review, *Constr. Build. Mater.*, 404, 133325(2023). https://doi.org/10.1016/j.conbuildmat.2023.133325

Wijesundara, S., Hemachandra, T., Bandara, S. and Wijesundara, K., Investigation of the shear capacity of ultra high-performance fiber reinforced concrete beams using machine learning techniques, *Struc. Infrastruc. Eng.*, 1-18(2025). https://doi.org/10.1080/15732479.2025.2521480

Yonggui, W., Shuaipeng, L., Hughes, P. and Yuhui, F., Mechanical properties and microstructure of basalt fibre and nano-silica reinforced recycled concrete after exposure to elevated temperatures, *Constr. Build. Mater.,* 247, 118561(2020). https://doi.org/10.1016/j.conbuildmat.2020.118561

Zakare, H., Alisibramulisi, A., Sidek, M. N. M., Newman, A., Saari, N., Adnan, S. H. and Bhkari, N. M., The Effect of Palm Oil Fuel Ash (POFA) and Steel Fiber Addition to the Mechanical Properties of Ultra High-Performance Concrete (UHPC), *Int. Conf. Sustain. Civ. Eng. Struc. Constr. Mater.,* 405-416(2020). https://doi.org/10.1007/978-981-16-7924-7_26

Zeyad, A. M., Agwa, I. S., Abd-Elrahman, M. H. and Mostafa, S. A., Engineering characteristics of ultra-high performance concrete containing basil plant ash, *Case Stud. Constr. Mater.*, 21, e03422(2024). https://doi.org/10.1016/j.cscm.2024.e03422

Zeyad, A. M., Agwa, I. S., Abd-Elrahman, M. H. and Mostafa, S. A., Engineering characteristics of ultra-high performance concrete containing basil plant ash, *Case Stud. Constr. Mater.*, 21, e03422 (2024). https://doi.org/10.1016/j.cscm.2024.e03422

Zheng, Y., Zhuo, J., Zhang, Y. and Zhang, P., Mechanical properties and microstructure of nano-SiO_2 and basalt-fiber-reinforced recycled aggregate concrete, *Nanotechnol. Rev.*, 11(1), 2169-2189(2022). https://doi.org/10.1515/ntrev-2022-0134